Chemical Imaging of Photoresists with Coherent Anti-Stokes Raman Scattering (CARS) Microscopy

Eric O. Potma and X. Sunney Xie

Department of Chemistry and Chemical Biology, Harvard University, 12 Oxford Street, Cambridge, Massachusetts 02138

Ligia Muntean, Jan Preusser,[†] David Jones, Jun Ye, and Stephen R. Leone*,[‡]

JILA, National Institute of Standards and Technology and University of Colorado, Department of Chemistry, and Department of Physics, Boulder, Colorado 80309-0440

William D. Hinsberg

IBM Almaden Research Center, 650 Harry Road, San Jose, California 95120-6099

Wolfgang Schade

Institute for Physics and Technology, Technical University Clausthal, 38678 Clausthal-Zellerfeld, Germany

Received: July 23, 2003

Coherent anti-Stokes Raman scattering (CARS) microscopy is demonstrated to be a powerful imaging technique with chemical specificity for studying chemically amplified polymer photoresists. Samples of poly(*tert*-butyloxycarbonyloxystyrene) (PTBOCST) resist imprinted by interferometric lithography with a pattern of lines/spaces of 400 nm/400 nm and 200 nm/200 nm were used to test CARS imaging capabilities. Chemical contrast in the image is obtained by probing the carbonyl stretching vibration of the *tert*-butoxyl carbonyl group of PTBOCST. The experimental images demonstrate high spatial resolution ($\approx$270 nm) and strong signal, which allows short acquisition times. Advantages and limitations of CARS in comparison with other imaging techniques with chemical specificity, such as infrared near field scanning optical microscopy (IR NSOM), are discussed.

I. Introduction

The continuing demand for higher performance integrated circuits places great importance on the development of advanced lithography. The most advanced lithographic technologies enable patterning of the resist materials with line dimensions below 100 nm,[1−5] which thus places new demands on measurement characterization techniques.

The process of accurately transferring a pattern to semiconductor surfaces by chemically amplified resist lithography consists of several steps and is still performed without a closed feedback procedure. Therefore, latent image metrologies are needed to characterize the evolution of the resist profile at various stages of image formation. First, an image of the pattern is generated on the photoresist by exposure to short-wavelength (typically UV) radiation. The pattern is created traditionally by a mask. For test patterns, interferometric lithography can be used to create a sinusoidal standing wave pattern produced by interference at the region of intersection of two coherent light beams.[6] An acid species is produced in the resist (an acid-labile polymer blended with a photoacid generator) only in the regions exposed to radiation, so that a first latent image is created. Chemically amplified resists operate by the mechanism of an acid-catalyzed reaction. This process takes place during a postexposure bake (PEB) at elevated temperatures when the acid interacts with multiple reaction sites to catalyze deprotection that alters the chemical and physical properties of the polymer. As a consequence, important changes in the vibrational spectrum of the polymer films are seen after the UV exposure and PEB. These changes provide a route to investigate polymer photochemistry and to measure line dimensions of latent images at this important intermediate stage in the image formation. The final step is the development of the latent image by dissolution of either the exposed (positive tone resists) or the unexposed (negative tone resists) areas and subsequent selective etching in the regions where the polymer was removed.

Confocal reflectance microscopy[7] has been used to characterize polymer photoresists with a resolution of hundreds of nanometers. However, reflectance microscopy is sensitive to topographical differences only. To examine the chemical conversion steps in the image formation process more directly, optical methods with chemical selectivity are preferred. Fluorescence microscopy offers chemically selective probing of the photoresists through specific labeling with pH sensitive dyes.[8,9] The drawback of this technique is that the required fluorophores possibly affect the parameters of acid diffusion and reactivity and, consequently, the line dimension and the line-edge roughness.

* To whom correspondence should be addressed. E-mail: srl@cchem.berkeley.edu.
† Current address: Institute for Physics and Technology, Technical University Clausthal, 38678 Clausthal-Zellerfeld, Germany.
‡ Current address: Department of Chemistry and Department of Physics and Lawrence Berkeley National Laboratory, University of California, Berkeley, CA 94720.

Imaging of Photoresists with CARS Microscopy

J. Phys. Chem. B, Vol. 108, No. 4, 2004 **1297**

Vibrationally sensitive microscopy circumvents labeling complications by making use of the changes in the polymer's vibrational spectrum. Infrared near field scanning optical microscopy (IR NSOM) has been employed to selectively probe the OH vibration produced upon UV exposure and PEB in certain resist systems.[10−13] Images with chemically specific absorption contrast have been obtained with a resolution of 300 nm at a wavelength of 3 μm (the OH stretching vibration) along with a simultaneous topographical characterization of the sample. To interrogate aspects of major importance for the control of the lithographic process such as acid diffusion and line-edge roughness, chemical imaging techniques with considerably higher spatial resolution are needed. In this respect, complementary X-ray and neutron reflectivity measurements have been used to measure the spatial evolution of the reaction−diffusion process with nanometer resolution.[14] These measurements provide a valuable test for any proposed simulation or model calculation for the reaction front propagation and can be used to validate different approaches quantitatively. However, as opposed to optical methods, the high experimental complexity of X-ray and neutron reflectance compromises the implementation of these nonoptical techniques when a rapid inspection of the photoresists is required.

Another promising optical method for studying the acid diffusion is apertureless near field scanning optical microscopy[15,16] used for infrared absorption contrast. So far, apertureless NSOM has been used in the visible for the photoresist systems providing high resolution (10 nm) in images where the contrast is given by changes in the refractive index.[17] Apertureless NSOM faces significant challenges for detecting the minute quantity of scattered light from the tip end in the presence of a large background. To alleviate this difficulty, polarization-based differential interferometric detection has been used.[18] In general, infrared absorption microscopy detects small changes on a large background, which compromises the signal-to-noise ratio. To enhance the sensitivity, background subtraction techniques such as lock-in detection can be used at the expense of image acquisition times ($>$15 min). Finally, the application of spontaneous Raman scattering microscopy for a rapid characterization of the films is limited by the low sensitivity of the technique. The low Raman scattering cross section necessitates long image integration times.

Here we explore the capabilities of coherent anti-Stokes Raman scattering (CARS) microscopy for the rapid characterization of polymer photoresists. CARS microscopy is an evolving technique that has been proven particularly useful for the imaging of living cells.[19−22] The much stronger signals in CARS microscopy yield images based on Raman contrast within tens of seconds. This fact also makes CARS one of the most promising imaging techniques for fast visualization of photoresists with chemical specificity. In particular, CARS microscopy shows the potential for real time investigations of the photochemistry in polymer photoresists at different stages of the lithographic process. In this study, we demonstrate the chemical sensitivity of CARS microscopy by visualizing line patterns in poly(*tert*-butyloxycarbonyloxystyrene) (PTBOCST) polymer photoresists.

II. CARS Microscopy

CARS microscopy is a nonlinear optical technique that is sensitive to the Raman vibrational activity of the specimen. In CARS, a pump beam with frequency ω_p and a Stokes beam with frequency ω_S are incident on the sample to drive a molecular vibration at a Raman shift of $\omega_0 = \omega_p - \omega_S$. A signal

is subsequently generated at the frequency $2\omega_p - \omega_S$. The CARS signal strength scales as

$$S_{CARS}(\omega_0) \propto |\chi_{CARS}^{(3)}(\omega_0)|^2 I_p^2 I_S \quad (1)$$

where I_p is the intensity of the pump and I_S the intensity of the Stokes beam. The nonlinear dependence of the CARS signal on the incident intensity favors signal formation only at the focus where the excitation density is the highest, giving CARS microscopy its 3D sectioning capability.[19,22] The total CARS excitation mechanism is a third-order process, the efficiency of which is given by the material property $\chi_{CARS}^{(3)}$, the third-order nonlinear susceptibility. The third-order susceptibility consists of a resonant part and a nonresonant part:[23]

$$\chi_{CARS}^{(3)}(\omega_0) = \chi_r^{(3)}(\omega_0) + \chi_{nr}^{(3)} \quad (2)$$

The resonant part accounts for the chemical selectivity of CARS, whereas the nonresonant part contributes a response that is virtually independent of the Raman shift ω_0 and gives rise to a nonresonant background in the CARS image. Here, both the glass support and the polymer film introduce a nonresonant signal. By substituting eq 2 into eq 1, the total CARS signal can be found to depend on the resonant and nonresonant contributions in the following manner:[23]

$$S_{CARS}(\omega_0) \propto |\chi_r^{(3)}(\omega_0)|^2 + 2\chi_{nr}^{(3)}\{Re\}\{\chi_r^{(3)}(\omega_0)\} + |\chi_{nr}^{(3)}|^2 \quad (3)$$

The first term is the resonant contribution to the signal, the second is a linear mixing term between the resonant and the nonresonant signal, and the last term is the constant nonresonant background. Only the first two terms contain chemically selective information. The nonresonant background can usually be determined independently by tuning away from the Raman transition ω_0 in order to minimize $\chi_r^{(3)}$. It is important to note that the CARS signal is not linear in the number of Raman scatterers. This is a result of the coherent property of CARS. Given that $\chi_r^{(3)}$ scales linearly with the number of vibrational modes, it can be seen that the first term in eq 3 depends quadratically on this number, whereas the linear mixing term shows a linear dependence on the number of Raman modes. A relative indication of the number densities in the image can be obtained by simply taking the square root of the total CARS signal.

The coherent property plays another important role in CARS microscopy. Contrary to spontaneous Raman microscopy, the CARS signal fields interfere with one another. This boosts the signal strength and determines the shape of the radiation profile.[22] In the forward propagation direction, the CARS light fields interfere constructively and yield signals much stronger than what can be attained in spontaneous Raman scattering microscopy. In the backward (epi) propagation direction, however, the wavevector mismatch comes into play and the degree of constructive interference depends on the size of the object.[22,24] Generally, the thicker the object, the more destructive interference. Objects or layers with a thickness much larger than the optical wavelength do not contribute to the epi-detected signal because of complete destructive interference. In this study, we utilize the CARS microscope in the epi-detection mode, which is insensitive to the nonresonant signal from the (thick) coverslip and only monitors features within about an optical wavelength from the polymer/air interface.

III. Experimental Methods

Two ps-Ti:sapphire lasers (Coherent, Mira 900, ~3.5 ps pulse width) are used to provide the pump and the Stokes beam,
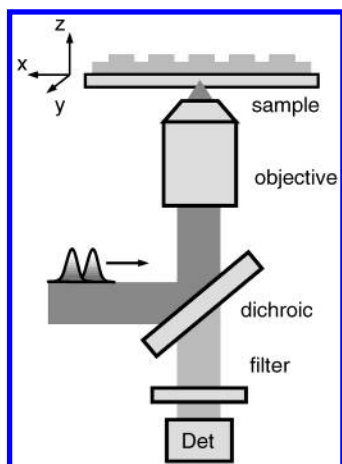
Figure 1. Layout of the CARS optical microscope and sample geometry.

Figure 2. Raman spectrum of the unexposed (a) and exposed (b) polymer film. Integration time was 150 s, and the background from the glass substrate has been subtracted. Spectra are smoothed with a 3-point 7th order polynomal interpolation procedure (Savitzky-Golay).

Figure 3. CARS signal of the unexposed film as a function of the Raman shift, relative to the nonresonant signal at 825 cm^{-1}. The Stokes beam was tuned while the pump beam remained fixed at 13 786 cm^{-1}.

respectively. To synchronize the 76 MHz pulse trains, the cavity length of the laser that delivers the pump is slaved to the cavity length of the Stokes laser (Coherent, Synchrolock). The time jitter between the pulses is less than 100 fs. Details on the laser system can be found elsewhere.[25,26] The pump beam was set to 13 786 cm^{-1} (725 nm), and the Stokes beam was varied between 12 838 and 12 958 cm^{-1} (771 to 778 nm). The laser outputs are filtered with color glass filters (RG 695) to remove the superradiance background at shorter wavelengths. The beams are spatially overlapped on a 50/50 beam splitter and directed into an inverted microscope (Nikon TE300). The average power for both beams was 10 mW before entering the microscope. Figure 1 illustrates the excitation and detection configuration of the microscope. A dichroic mirror (Chroma, 700dcspxr) reflects the incident beams into a 1.4 NA oil immersion objective (Nikon, Plan apo). The diameter of the beams is expanded to overfill the back aperture of the objective. The sample is scanned with a pzt-driven stage scanner. The CARS signal is collected in the backward (epi-) direction and separated from the incident beams by the dichroic mirror. A stack of 3 band-pass filters (Coherent, 670 nm) is used to suppress any incident radiation at the detector stage (single photon avalanche photodiode).

An estimate of the spatial resolution of the CARS microscope is obtained by scanning 175 nm polystyrene beads through the focus. The beads are visualized through the 1040 cm^{-1} aromatic ring vibration. A resolution of 270 nm in the lateral direction and 660 nm along the axial coordinate is determined.

Raman spectra are recorded with a confocal Raman microspectrometer (Jobin Yvon, Labram). A 0.9 NA air objective is used to focus 15 mW of 632 nm light onto the sample. Signal integration times amount to 150 s per spectrum.

Photoresist samples consist of poly-*t*-butyl oxistyrene (PTBOCST) layers spin-coated onto borosilicate glass coverslips. The photoacid generator (PAG) in the resist is bis(*tert*-butyl-phenyliodonium)perfluoro-*n*-octane sulfonate at a concentration of 0.0445 molal. Film thickness is ~1200 nm. The periodic line pattern is produced by interferometric lithography by illuminating with 257 nm light at a dose of 10 mJ/cm^2. The nominal line widths of the two patterns are 400 and 200 nm. The films are postapply baked at 130 °C for 60 s and post-exposure baked at 100 °C for 60 s. Under acidic conditions, the *tert*-butyl carbonyl group of PTBOCST is converted to a hydroxy group with release of carbon dioxide and nominally iso-butylene, although other volatile products can be produced. This forms the basis of the chemical contrast of the pattern.
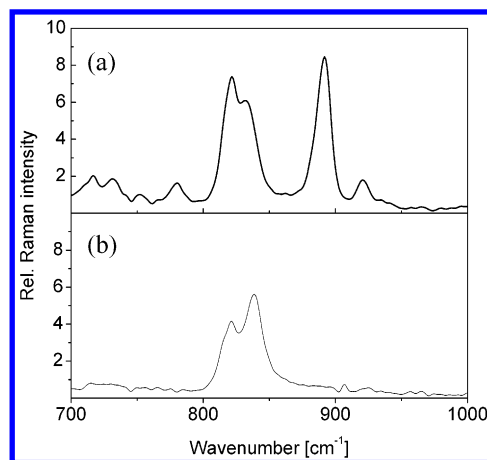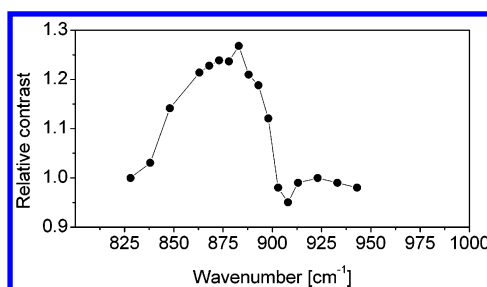
The release of the reaction byproducts in the exposed regions causes the polymer to shrink, generating a topographical pattern.

IV. Results

Figure 2 shows the Raman spectra of the photoresist before and after UV illumination in the region from 700 to 1000 cm^{-1}. In this region, a prominent change is observed upon UV exposure. The band at 891 cm^{-1}, which can probably be assigned to a *tert*-butoxyl skeletal mode, disappears after the photoconversion of the polymer.

The CARS signal bears a similar sensitivity to the *tert*-butoxyl skeletal mode. In Figure 3, the observed CARS spectral contrast for the unexposed polymer film is given. Other than the Raman signal, the detected CARS signal contains a background contribution. Interference of vibrationally resonant features with the nonresonant background gives rise to generally broader line shapes, which carry a dispersive contribution. This explains the larger width and the relative red-shift of the CARS spectral profile.

The spectral sensitivity of the CARS microscope to the skeletal vibration allows one to generate images of the photoresist with chemical contrast. Figure 4a depicts an image of a PTBOCST polymer film that has been patterned with a line/space pattern of 400 nm/400 nm. The sample is scanned axially and laterally through focus yielding an *xz* cross-section through the polymer film. The image is taken at a Raman shift of 880 cm^{-1} and is composed of both the resonant and the nonresonant signal contribution. The nonresonant signal can be separately visualized by tuning the Raman shift away from the *tert*-butoxyl vibration. This is displayed in Figure 4b, in which the same region has been imaged at 925 cm^{-1}. The signal originates from
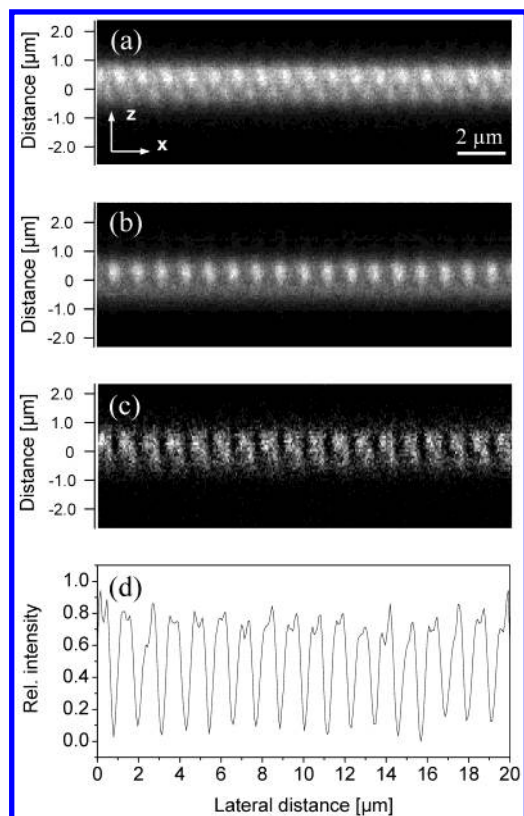
Imaging of Photoresists with CARS Microscopy

J. Phys. Chem. B, Vol. 108, No. 4, 2004 **1299**

Figure 4. epi-CARS images of the patterned TBOC film. The sample was scanned axially and laterally through focus yielding a *xz* cross-section of the polymer film at a Raman shift of 880 cm^{-1} (a) and 925 cm^{-1} (b). Images are 20.0 × 5.0 μm (*x,z*) and consist of 256 × 64 pixels. The dwell time is 0.3 ms. The difference image (a and b) is given in (c), along with a one-dimensional integration of image (c) along the *z* axis, the result of which is given in (d).
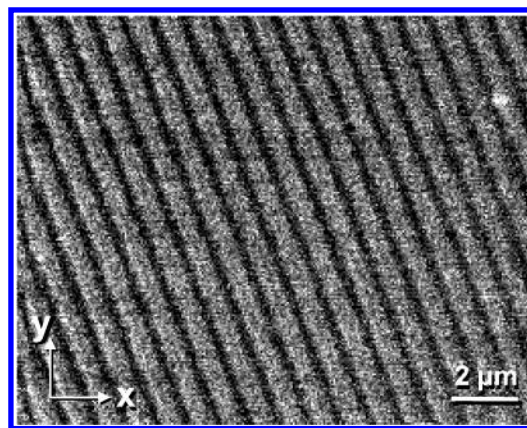

Figure 5. EpiCARS difference-image of patterned TBOC film in the lateral plane (*x,y*). The image was obtained after subtracting an image taken at 925 cm^{-1} from an image recorded at 880 cm^{-1} with pixel dwell time of 0.3 ms. Image measures 20.0 × 15.6 μm (*x,y*) and consists of 256 × 200 pixels.

the forward propagating nonresonant signal generated in the glass and in the polymer film, which is subsequently back-reflected at the polymer/air interface into the epi-direction. Differences in $\chi_{nr}^{(3)}$ and the thickness of the exposed and unexposed areas in the polymer give rise to contrast in the image. In addition, the topographic characteristics of the PTBOCST film and the difference in refractive index of the exposed and unexposed regions modulate the efficiency of back reflection, which is another source of image contrast. Importantly, the image shown in Figure 4b contains no direct chemically specific information, because the nonresonant signal exhibits no significant dependence on the Raman shift.

Although the nonresonant signal is strong, a chemically selective image can be obtained by subtracting Figure 4b from Figure 4a. The result is given in Figure 4c. The chemical pattern is now clearly recognized, with the bright zones indicating the unexposed regions of the polymer film that contain the *tert*-butoxyl skeletal mode. The regions exposed to UV radiation show up as the gaps. Note that the contrast observed in the difference image results solely from the spectral differences of the resonant contribution to the CARS signal as the nonresonant signal exhibits a virtually flat spectral dependence.[23] For example, subtracting images taken at 825 cm^{-1} from corresponding signals measured at 925 cm^{-1} yields featureless images. From the difference image in Figure 4c, it is determined that the chemically selective signal contributes 21% (±3%) to the total image intensity, whereas the nonresonant background accounts for the remaining 79% (±3%).

A one-dimensional cross section of the difference-image, obtained by integrating Figure 4c along the *z* dimension, is given

in Figure 4d. Because the depth of the imprinted pattern compares to the resolution depth of the CARS microscope, a one-dimensional projection by integrating along the *z* coordinate is expected to retain all of the spatial features of the photoresist. It can be clearly seen that the photo treatment and the chemical changes during the high-temperature bake have imprinted lines of nominal width of ~350 nm in the photoresist. The peaks exhibit flat tops, whereas the dips are much sharper. This results in an apparent duty cycle of the pattern that deviates somewhat from the 50:50 duty cycle of the illumination pattern, which is also apparent in Figure 4c. From Figure 4d, it is furthermore seen that the CARS signals at the edges of the unexposed/exposed interface are greater than the center regions corresponding to the unexposed regions. Similar edge enhancement has also been observed with infrared NSOM[11] and atomic force microscopy[27] and has been reported to be a topographical effect (of the order of a couple of nanometers[27]). It has been attributed to the shrinkage of the polymer probably due to an edge effect but has not been clarified yet.[11,27] Different methods of exposure of the radiation have been used in each of these cases, such as UV exposure through a mask,[8] electron beam writing,[24] and exposure to the interference of two UV beams for the samples studied here. This fact suggests that this topographical structure appears to occur during the postexposure bake time. However, a difference of a few nanometers is not expected to give such a significant modulation of the CARS signal. We have observed similar enhancements near the edges of 1 μm polystyrene beads in E-CARS images (data not shown). The E-CARS microscope is particularly sensitive to an asymmetric distribution of scatterers in the focus,[22] such as is the case near the edge, which might account for the edge enhancement seen in the photoresist images.

The usefulness of the CARS microscope for rapid pattern characterization is illustrated by the difference-image of a photoresist in the *xy* plane, shown in Figure 5. The sample is identical to the sample in Figure 4. The image results after subtracting separately recorded images at 880 and 925 cm^{-1}, respectively. Each image was taken with an acquisition time of 17 s. For comparison, a similar image based on spontaneous Raman scattering contrast would have taken more than an hour. The difference-image reveals, with a high spatial resolution, the chemical pattern of the 400 nm line spacing in the polymer photoresist. The high spatial resolution of CARS microscopy allows visualization of even finer patterns. Figure 6 shows a line scan of a PTBOCST film that has been radiated with a
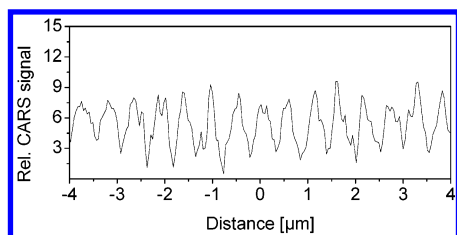
Figure 6. Integrated line scan of a TBOC photoresist patterned with a 200 nm line spacing. The profile was obtained after subtracting the constant nonresonant background recorded at 925 cm^{-1} from a line scan taken at 880 cm^{-1}. The graph is obtained after integration of a cross-section through the layer in 40 steps, similar to Figure 4d. The total acquisition time is 10 s.

pattern of 200 nm line spacing. In imaging such fine structures, sharp features are lost because the resolution of the microscope is close to the spatial separation of the irradiated lines. We attribute the nonuniformity of the duty cycle to the lower signal-to-noise than was obtained in Figure 4d. Nevertheless, the chemical imprint can be clearly recognized, which enables inspection of systematic patterns at even these small spatial scales.

V. Discussion

In this study, we have used CARS microscopy as a potential technique for investigating UV lithographic patterns in polymer photoresists. CARS microscopy offers several advantages over existing optical techniques for characterizing polymeric photoresists. Similar to IR NSOM and spontaneous Raman microscopy, the chemical selectivity of the CARS microscope allows inspection of the photochemically imprinted image without the use of fluorescent contrast agents. Among these vibrationally sensitive techniques, spontaneous Raman microscopy is experimentally the least demanding but yields weak signals and long acquisition times. Also IR NSOM and IR apertureless NSOM suffer from long signal integration times to reach sufficient signal-to-noise in the images. The much stronger signals in CARS microscopy, on the other hand, reduce the scanning time to tens of seconds with the potential of a few seconds per image if beam scanning methods are used. This implies that samples can be rapidly inspected, which is attractive for high throughput screening. In addition, the faster imaging permits recording of dynamic changes in the photochemistry of the resist during the different stages of the patterning process. Another advantage of CARS microscopy relative to IR aperture probe NSOM and IR apertureless NSOM is the lack of tip−sample interaction. The high spatial resolution of CARS microscopy compares with confocal Raman microscopy and IR NSOM, and it reveals fine contrast down to ∼200 nm. In contrast, the IR apertureless NSOM technique can achieve higher spatial resolution than CARS (≈10 nm versus ≈270 nm), but it is limited by the quality of infrared laser sources, the challenge of detecting the minute amount of signal that is inherent to the method's principle, and by less sensitive detectors. CARS microscopy can be used to perform depth profiling measurements, similar to confocal microscopy.

In visualizing periodically modulated surfaces, Fresnel diffraction effects might alter the final image when the spatial extent of the periodic modulation is smaller than the resolution of the microscope.[28,29] We have observed such problems when operating the microscope in the confocal reflectance mode, in which ghost images can appear due to grating effects. The contrast in CARS microscopy has a different origin. The epi-CARS signal at the polymer/air interface results from differences in both $\chi^{(3)}$ and linear refraction contributions.[22] Contrary to the photoresist images acquired through confocal microscopy, we have not observed any signs of Fresnel diffraction effects in the CARS images.

The presence of a nonresonant background complicates measurements with the CARS microscope. In the epi-detection mode of the microscope, the background arises predominantly from the nonresonant signal generated in the polymer bulk that is back-reflected at the polymer/air interface. The nonresonant background can be entirely suppressed when polarization selective detection is employed.[30] In polarization CARS (P−CARS), the difference in the polarization of the nonresonant and resonant signal contributions is utilized to block out the nonresonant part with a crossed polarizer, while a portion of the resonant signal is passed on to the detector. However, the more complicated detection geometry and the low signal yield in P−CARS make the epi-CARS method preferable for inspection of patterned polymer films. In this study, we have simply subtracted the nonresonant background by tuning the frequency away from the Raman resonance. Using background subtraction, chemically selective images can be easily obtained despite the presence of a strong nonresonant background. The resulting images reveal the fine structure of the chemical pattern at a high spatial resolution. An additional laser beam of a different frequency could potentially be used to record a nonresonant background image simultaneously with the resonant image, thereby decreasing the total acquisition time even further.

In conclusion, the vibrational sensitivity of the CARS microscope allows visualization of the polymeric photoresists with chemical contrast. CARS microscopy exhibits a high spatial resolution and enables fast image acquisition rates. Both of these aspects are key in investigating chemically amplified polymer photoresists, promoting CARS as a potentially powerful technique for studying these systems.

References and Notes

(1) Canning, J. *J. Vac. Sci. Technol. B* **1997**, *15*, 2109.
(2) Silverman, J. *J. Vac. Sci. Technol. B* **1997**, *15*, 2117.
(3) McCord, M. *J. Vac. Sci. Technol. B* **1997**, *15*, 2125.
(4) Harriott, L. *J. Vac. Sci. Technol. B* **1997**, *15*, 2130.
(5) Gross, G. *J. Vac. Sci. Technol. B* **1997**, *15*, 2136.
(6) Hinsberg, W.; Houle, F. A.; Hoffnagle, J.; Sanchez, M.; Walraff, G.; Morrison, M.; Frank, S. *J. Vac. Sci. Technol. B* **1998**, *16*, 3689.
(7) Zhang, P. L.; Webber, S.; Mendenhall, J.; Byers, J.; Chao, K. in *Proc. SPIE* **1998**, *3333*, 794−805.
(8) Dentiger, P. M.; Lu, B.; Taylor, J. W.; Bukofsky, S. J.; Feke, G. D.; Hessman, D.; Grober, R. D. *J. Vac. Sci. Technol. B* **1996**, *14*, 4239.
(9) Lu, B.; Taylor, J. W.; Cerrina, F.; Soo, C. P.; Bourdillon, A. J. *J. Vac. Sci. Technol. B* **1999**, *17*, 3345.
(10) Dragnea, B.; Leone, S. R. *J. Appl. Phys* **1999**, *86*, 2795.
(11) Dragnea, B.; Preusser, J.; Szarko, J. M.; McDonough, L. A.; Leone, S. R. *Appl. Surf. Sci.* **2001**, *19*, 783.
(12) Dragnea, B.; Preusser, J.; Szarko, J. M.; Leone, S. R.; Hinsberg, W. D. *J. Vac. Sci. Technol. B* **2001**, *19*, 142.
(13) Dragnea, B.; Leone, S. R. *Int. Rev. Phys. Chem.* **2001**, *20*, 59.
(14) Lin, E. K.; Soles, C. L.; Goldfarb, D. L.; B. C.Trinque; Burns, S. D.; Jones, R. L.; Lenhart, J. L.; Angelopoulos, M.; Wilson, C. G.; Satija, S. K.; Wu, W. L. *Science* **2002**, *297*, 372−375.

Imaging of Photoresists with CARS Microscopy

J. Phys. Chem. B, Vol. 108, No. 4, 2004 **1301**

(15) Zenhausern, F.; O'Boyle, M. P.; Wickramasinghe, H. K. *Appl. Phys. Lett.* **1994**, *65*, 1623.

(16) Knoll, B.; Keilmann, F. *Nature* **1999**, *399*, 134.

(17) Preusser, J. Private communication.

(18) Wickramasinghe, H. K. *Opt. Eng.* **1985**, *24*, 926.

(19) Zumbusch, A.; Holtom, G. R.; Xie, X. S. *Phys. Rev. Lett.* **1999**, *82*, 4142.

(20) Potma, E. O.; Boeij, W. P. d.; Haastert, P. J. M. v.; Wiersma, D. A. *Proc. Natl. Acad. Sci. U.S.A.* **2001**, *98*, 1577.

(21) Cheng, J. X.; Yia, Y. K.; Zheng, G.; Xie, X. S. *Biophys. J.* **2002**, *83*, 502.

(22) Cheng, J. X.; Volkmer, A.; Xie, X. S. *J. Opt. Soc. Am. B* **2002**, *10*, 1363.

(23) Eesley, G. L. *Coherent Raman Spectroscopy*; Pergamon Press: New York, 1981.

(24) Volkmer, A.; Cheng, J. X.; Xie, X. S. *Phys. Rev. Lett.* **2001**, *87*, 023901.

(25) Potma, E. O.; Jones, D. J.; Cheng, J. X.; Xie, X. S.; Ye, J. *Opt. Lett.* **2002**, *27*, 1168.

(26) Jones, D. J.; Potma, E. O.; Cheng, J. X.; Burfeindt, B.; Pang, Y.; Ye, J.; Xie, X. S. *Rev. Sci. Inst.* **2002**, *73*, 2843.

(27) Ocola, L. E.; Fryer, D. S.; Reynolds, G.; Krasnoperova, A.; Cerrina, F. *Appl. Phys. Lett.* **1996**, *68*, 717.

(28) Sheridan, J. T.; Körner, T. O. *J. Microsc.* **1994**, *177*, 95.

(29) Testorf, M.; Ojeda-Castaneda, J. *J. Opt. Soc. Am. A* **1996**, *13*, 119.

(30) Cheng, J. X.; Book, L. D.; Xie, X. S. *Opt. Lett.* **2001**, *26*, 1341.